





Independently tunable metamaterial inspired compact triband dual-sense circularly polarized antenna

Vinaya Kumar Sugganapalya Rajanna^{1,2} , T. Venkatesh³,
Puneeth Kumar Tharehalli Rajanna⁴  and Shambulinga Mudukavvanavar⁵

Research Paper

Cite this article: Rajanna VKS, Venkatesh T, Tharehalli Rajanna PK, Mudukavvanavar S (2024) Independently tunable metamaterial inspired compact triband dual-sense circularly polarized antenna. *International Journal of Microwave and Wireless Technologies*, 1–9. <https://doi.org/10.1017/S1759078724001247>

Received: 24 July 2024
Revised: 9 November 2024
Accepted: 18 November 2024

Keywords:

Slot antenna; axial ratio; circular polarization; split ring resonator

Corresponding author: Vinaya Kumar Sugganapalya Rajanna;
Email: svinayssit@gmail.com

¹Electrical and Electronics Engineering, Ghousia College of Engineering, Ramanagara, Karnataka, 590018 India; ²India Affiliated to Visvesvaraya Technological University, Belgaum, Karnataka, 590018; ³Computer Science and Engineering, Ghousia College of Engineering, Ramanagara, Karnataka, India; ⁴Electronics and Telecommunication Engineering, Siddaganga Institute of Technology, Tumkur, Karnataka, India and ⁵Electronics and Telecommunication Engineering, RV College of Engineering, Bangalore, Karnataka, India

Abstract

In this article, a dual-sense triband circularly polarized modified slot antenna loaded with metamaterial structures such as split-ring resonator and cross strips is proposed. The first resonant frequency is generated using the modified square slot which produces the two degenerative modes required to achieve circular polarization (CP). The corners of slot antenna are extended to obtain the orthogonal modes. The second resonant band is obtained using the single split-ring resonator. Two micro-splits in Split Ring Resonator (SRR) orthogonal to each other produces CP due to electric field generated by the micro-splits. The third resonance band is obtained due to loading of cross strips. The orthogonal phase is adjusted by varying the length of cross strips, so that the CP is achieved. All resonance bands are tuned independently. The measured impedance bandwidth of 31.68%, 4.55%, and 8.6% is obtained in first, second, and third bands respectively. The axial ratio bandwidth of 13.04%, 2.7%, 8.6% and peak gain of 3.8 dBic, 3.9 dBic, 3.7 dBic are obtained respectively. The simulated radiation efficiencies of above 80% is achieved in all bands. The left-hand CP is obtained in first two band as co-polarization and right-hand CP is obtained at the third band as co-polarization with respect to cross-polarization radiation. The cross-polarization of minimum -10 dB is obtained in all three bands. The proposed design is well suitable for the Bluetooth, n78 and n79 5G applications.

Introduction

Nowadays, due to increase in the demand of wireless components such as antennas, which are compact devices with low profile are very much essential with good performance. Compact antennas required to work at multiple frequencies with good isolation and provide ease of tuning between frequency bands. Many designs are available to obtain dual band [1, 2], triband, and multiple bands. In paper [3], a dual-band antenna with tri-polarization is obtained using slotted patch technique. Triple-band antennas are essential in few applications which work simultaneously at three resonant frequencies are proposed in papers [4]–[6]. A few designs on multiband antennas are proposed in papers [7]–[10] which are essential in wireless applications. Recently, many multiband designs are proposed for Ultra Wideband (UWB) applications [11], mobile handsets [12], and fast redesign method for wireless application [13]. Also independently tuned frequency bands are proposed using diodes [14, 15]. Above designs possess linear polarization (LP) which requires perfect line of sight for better signal reception, but circular polarization (CP) has advantageous than LP in terms of orientation, interference, fading, and immune to noise. So CP antennas are much essential in wireless applications. A few CP designs are proposed to cover dual band [16], triband [17], and multiband [18, 19] used in different applications. All these designs are not capable of tuning frequency bands, but a few antennas are designed to achieve frequency reconfigurability [20]–[22] and independent tuning of frequency bands [23, 24]. PIN diodes and varactor diodes are used to obtain reconfigurability and independent tuning capability, but the design requires complex fabrication and external circuit. A few metamaterial-based designs are proposed to achieve dual- and triple-band operation with independent tuning, which provides ease of fabrication. These designs produces LP [25] and CP [26]–[28], but they uses multiple strips

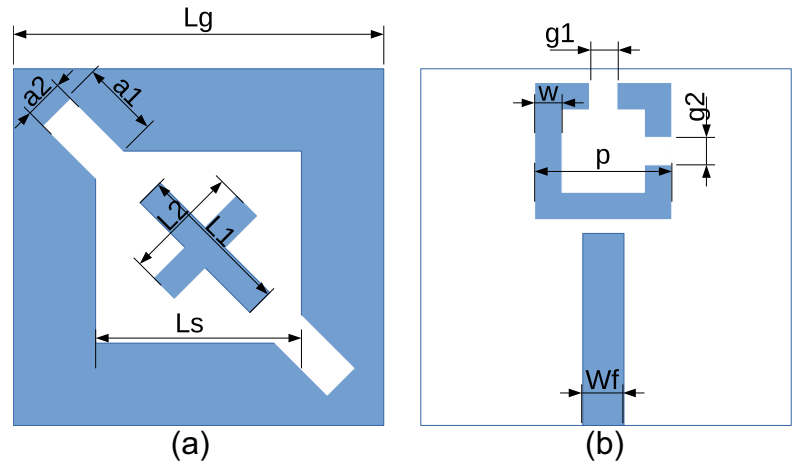


Figure 1. Antenna geometry. (a) Front view and (b) Back view. $L_g = 50$ mm, $a_1 = 8$ mm, $a_2 = 4$ mm, $L_1 = 20$ mm, $L_2 = 18$ mm, $L_s = 36$ mm, $W_f = 3.1$ mm, $L_f = 25$ mm, $p = 18$ mm, $w = 2$ mm, $g_1 = 1.2$ mm, $g_2 = 1.4$ mm.

and SRRs to achieve desired result. In the proposed design, a compact antenna with single strip SRR and two cross strips provide the intended result with good axial ratio bandwidth (ARBW).

In this paper, a single SRR and cross strips loaded circular polarized modified slot antenna is designed and validated through experiment. The slot antenna is modified in its corner to provide CP in first band. The corner expansion method provides two degenerative modes required to produce CP. Second band is generated due to loading of single SRR. A dual split produce orthogonal electric field to obtain CP. The third band is obtained through the asymmetric length cross strips. By varying the length of strips, orthogonal phase is achieved to obtain CP. All bands are tuned independent to each other. The sense of polarization is LHCP (left-hand circular polarization) for first two bands and RHCP (right-hand circular polarization) for third band. These polarization sense also can be tuned by changing the orientation of individual element.

Design principle

The proposed triband antenna is shown in Fig. 1. The front and back views are shown in Fig. 1(a) and (b). The modified slot is etched in the front side of the ground plane and cross strips are placed. The microstrip line is used for excitation and it is etched on the backside. The SRR is placed at a distance of 2 mm from the feed line. The substrate material used for the design is Rogers 4003C ($\epsilon_r = 3.38$, $\tan\delta = 0.009$). The dimensions of the antenna are provided in Fig. 1.

Triple-band operation

The mechanism for obtaining the triband operation is described in Fig. 2. Figure 2(a) shows the resonance obtained due to the square slot. The resonance frequency of slot antenna is obtained using Equation (1). The second band is achieved due to the asymmetric micro-split SRR and its surface current is shown in Fig. 2(b). Finally the third band is obtained using the cross strips and its surface current is shown in Fig. 2(c). The electric field of microstrip line excites the slot and cross strips. The slot and two strips are maximally coupled and produce the corresponding resonant frequency. The positioning of strips are 45° with respect to x -axis. The axial magnetic field excites the SRR. The proper orientation and position gives maximum coupling, which is modeled as LC resonant circuit and provide resonance

$$f_r = \frac{c}{2L_s} \sqrt{\frac{2}{1 + \epsilon_{eff}}} \quad (1)$$

where ϵ_{eff} is the effective dielectric constant.

The equivalent circuit of the proposed design is shown in Fig. 3(a). It consists of slot resonance which has shunt LC circuit. The energy coupling from slot excites the strips and SRR which is shown by mutual coupling in the circuit. The strips comprises of LC circuit which provides resonance due to current flow in the strips. The current flow gives inductance and the capacitance is in parallel with inductance due to separation of dielectric from strips and ground plane. The SRR has magnetically coupled from slot which has current flow in the loop of SRR. The current flow in SRR loop provides inductance and the capacitance is obtained due to multiple splits in the SRR. The values of inductance and capacitance are calculated using well-known resonance equation and provided in Fig. 3. The simulation of equivalent circuit is carried out using ADS simulator and the performance of S_{11} is compared with Electromagnetic (EM) simulation. The S_{11} performance of circuit and EM simulation is well in agreement and it is shown in Fig. 3(b). The values of optimized lumped elements are given by $R = 4.41$ k Ω , $L_1 = 0.31$ nH, $C_1 = 6.06$ pF, $L_2 = 0.26$ nH, $C_2 = 3.89$ pF, $L_3 = 0.94$ nH, $C_3 = 4.9$ pF.

CP mechanism

The mechanism of obtaining CP in each band is described here. The first band is obtained due to square slot antenna. The square slot is extended in its corner to obtain two degenerative modes. The extended slots are optimized to get the orthogonal modes which are required for CP. The second band is achieved using a single SRR with dual micro-splits. The splits are in asymmetric gaps which produces the orthogonal electric fields, that intern generates CP. The third band is obtained by loading the cross strips on the slot. By varying the length and width of the strips, CP is obtained. Here the sense of polarization of third band is RHCP, while first and second band is LHCP. Here the electric field or surface current distribution is shown with respect to $+z$ direction, so that the dual-sense polarization is seen. To validate the antenna resonates CP due to each of the individual structure, the electric field and surface current distribution is shown in Fig. 4. In the figure, Fig. 4(a) and (b), the electric field distribution of modified slot is seen, the field vectors rotate in the clockwise direction toward $+z$ -axis producing

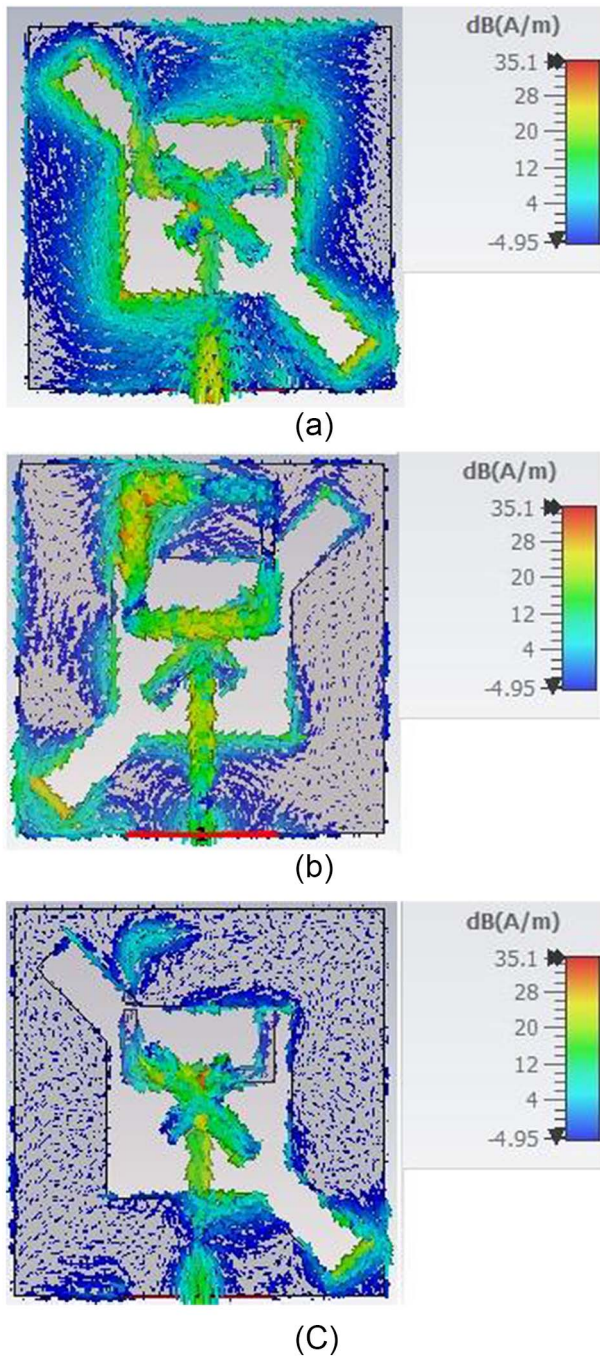


Figure 2. Surface current distribution on (a) modified slot, (b) cross strips, and (c) SRR.

the LHCP. Figure 4(c) and (d) depicts the electric field distribution of SRR in $-z$ direction and field vector rotates in anticlockwise direction producing LHCP. Figure 4(e) and (f) shows the surface current on the cross strips, which rotates vector anticlockwise in $+z$ direction producing RHCP radiation. The sensitive parameters and independent tuning capability are found using the parametric variation. Figure 5(a) shows reflection coefficient of the slot variation, while keeping other structures constant. It shows that when the length of square slot is varied, there is a change in the resonance and axial ratio values. If the slot dimension increases, the resonance shifts toward lower frequency and if slot dimension decreases the

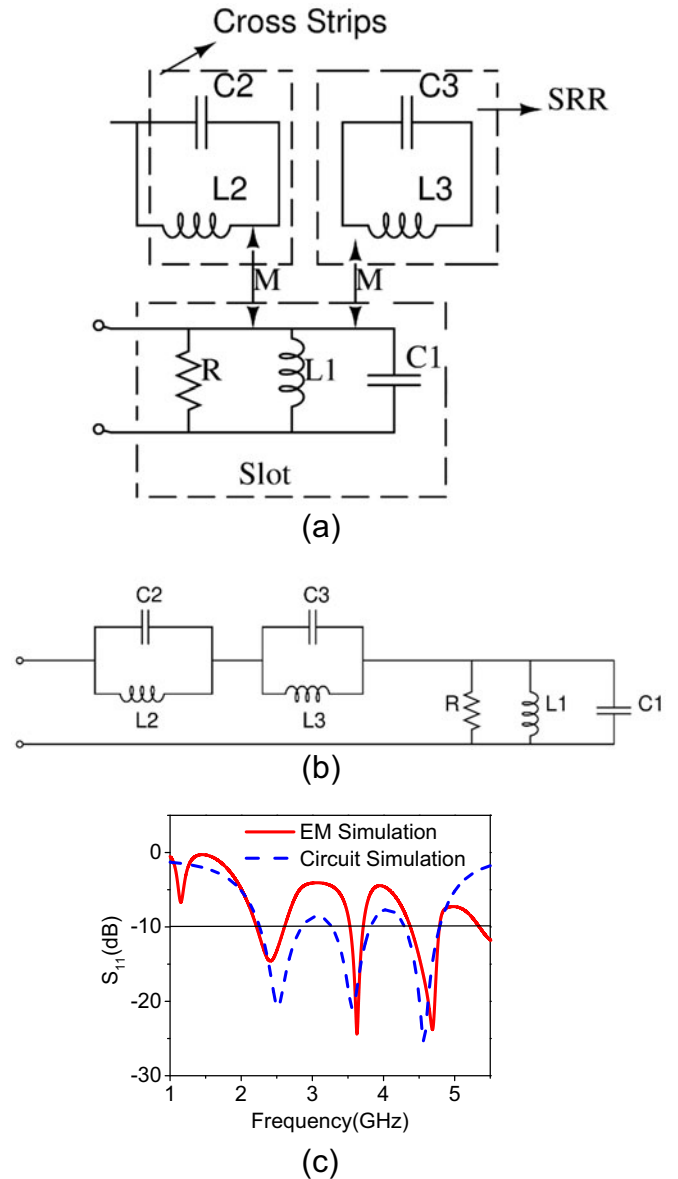


Figure 3. (a) Equivalent circuit of energy coupling form slot to strips and SRR, (b) equivalent circuit of proposed design, and (c) S_{11} comparison between EM and circuit simulation.

resonance shifts toward higher frequency. The axial ratio plot is shown in Fig. 5(b). Similarly, the second resonance can be tuned using SRR dimension. The length of the SRR is varied and its corresponding changes in S_{11} and axial ratio can be seen in Fig. 5(c) and (d). In the third resonance, tuning is obtained due to variation in the length of each strips. The tuning of S_{11} and axial ratio plots of cross strips are observed in Fig. 5(e) and (f). From this parametric tuning, it is concluded that the dimension can be varied individually to tune the frequency bands independently without affecting the other frequency bands.

Results and discussion

The proposed structure is fabricated and shown in Fig. 6. The design is experimentally validated using Vector Network Analyzer (VNA) and anechoic chamber. Figure 6(a) shows the front view,

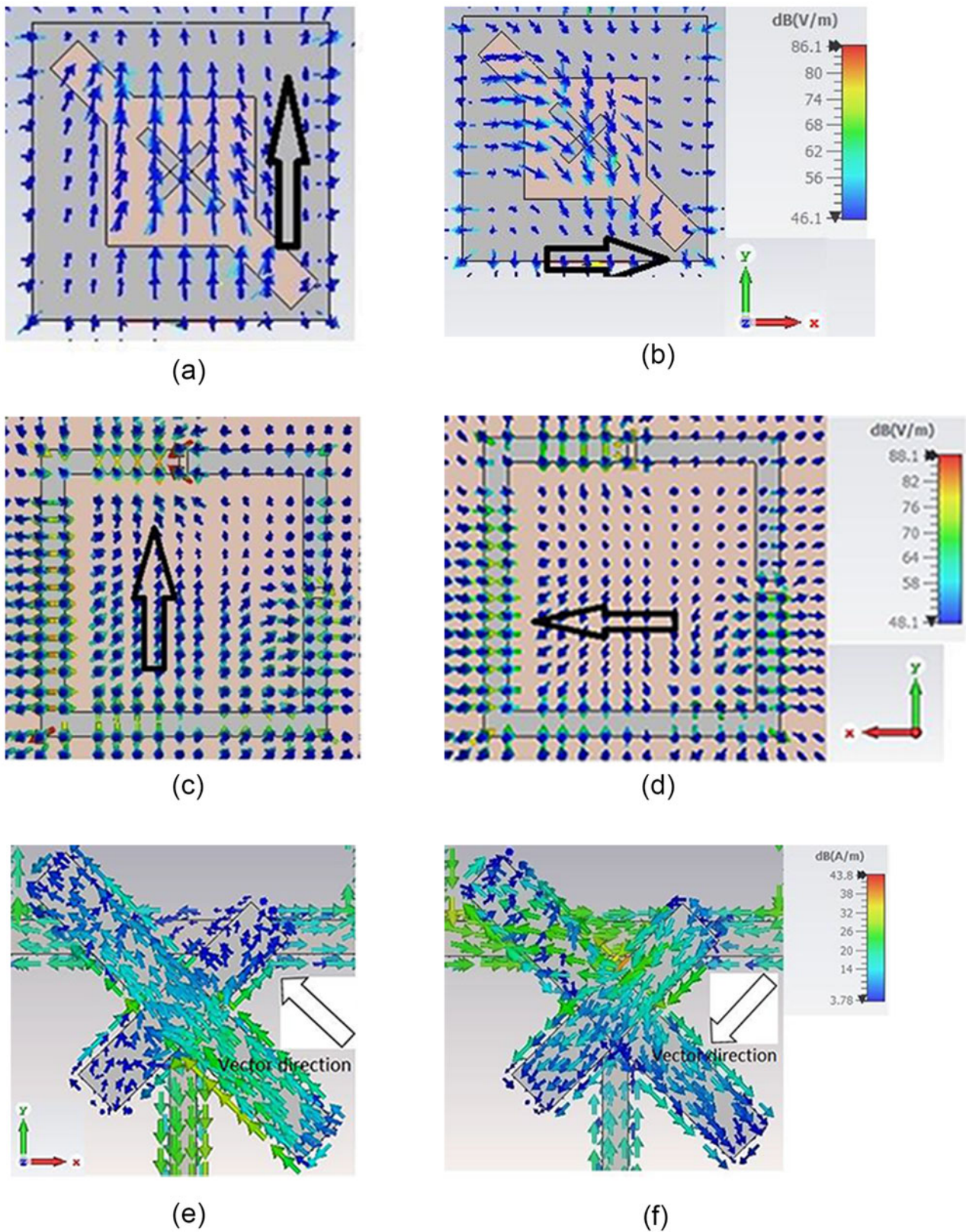


Figure 4. Electric field distribution of slot at (a) $\omega t = 0^\circ$ and (b) $\omega t = 90^\circ$, electric field distribution of SRR at (c) $\omega t = 0^\circ$ and (d) $\omega t = 90^\circ$, and surface current distribution of cross strips at (e) $\omega t = 0^\circ$ and (f) $\omega t = 90^\circ$.

Fig. 6(b) shows the back view, Fig. 6(c) depicts the experimental setup to measure S_{11} , and Fig. 6(d) shows the picture of measuring various parameters in the anechoic chamber. The 50Ω

Sub Miniature Version A (SMA) is used as connector for feeding the input power. The impedance bandwidth obtained in the simulation for all three frequency bands are 15.76%, 4.68%, and

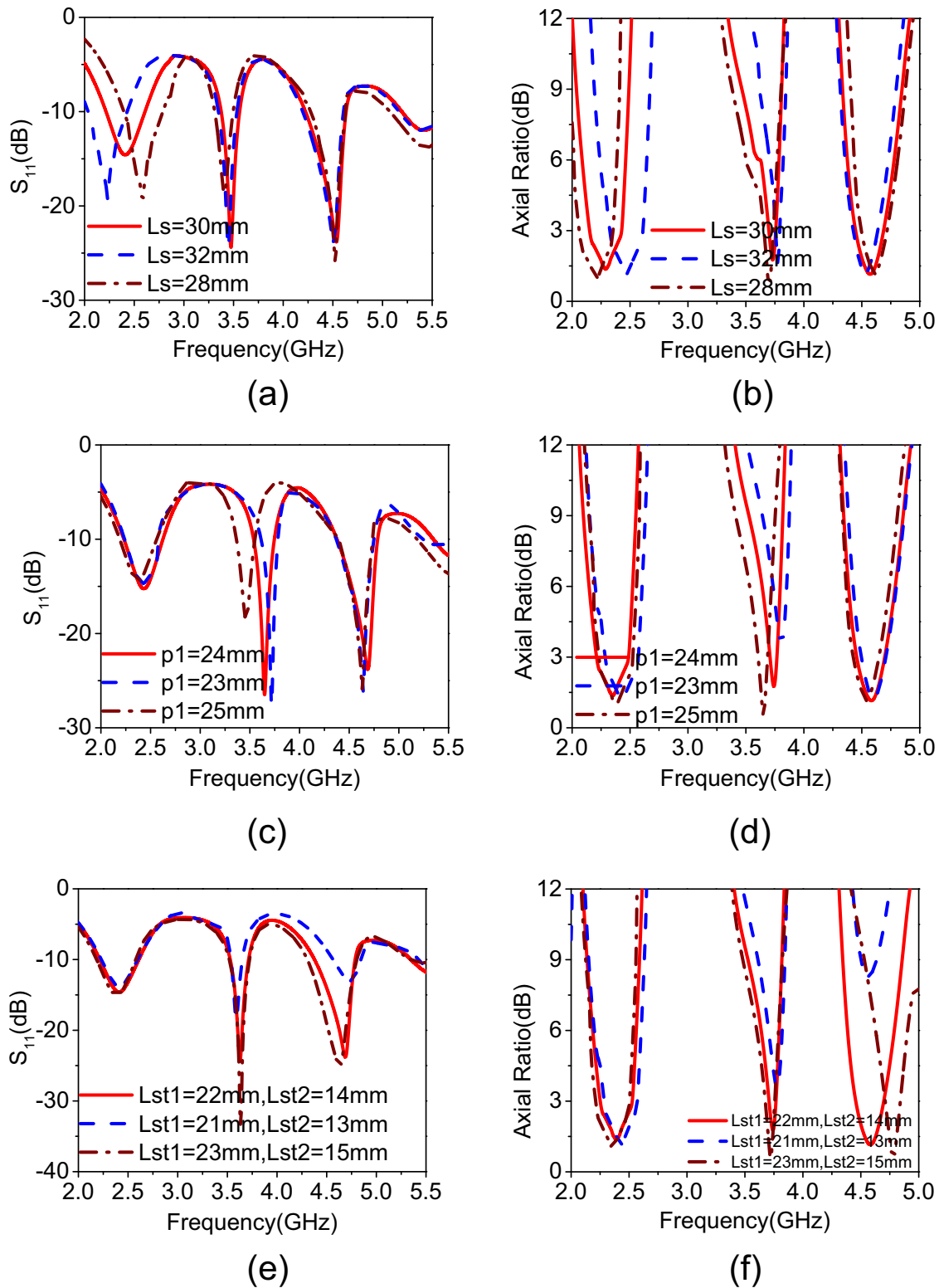


Figure 5. Parametric variation of slot antenna, SRR, and cross strips: (a) S_{11} (L_s variation), (b) axial ratio (L_s variation), (c) S_{11} due to p_1 , (d) AR due to p_1 , (e) S_{11} (variation of L_{st1} and L_{st2}), and (f) AR (variation of L_{st1} and L_{st2}).

8.07%. The measured impedance bandwidth are 31.68%, 4.55%, and 8.6%. Figure 7(a) shows the comparison between simulated and measured data of S_{11} . The simulated ARBW of 12.5%, 2.73%,

and 6.66% is obtained in each band. The measured ARBW of 13.04%, 2.7%, and 8.6% is well correlated with simulated values at each frequency band and it is shown in Fig. 7(b). The simulated

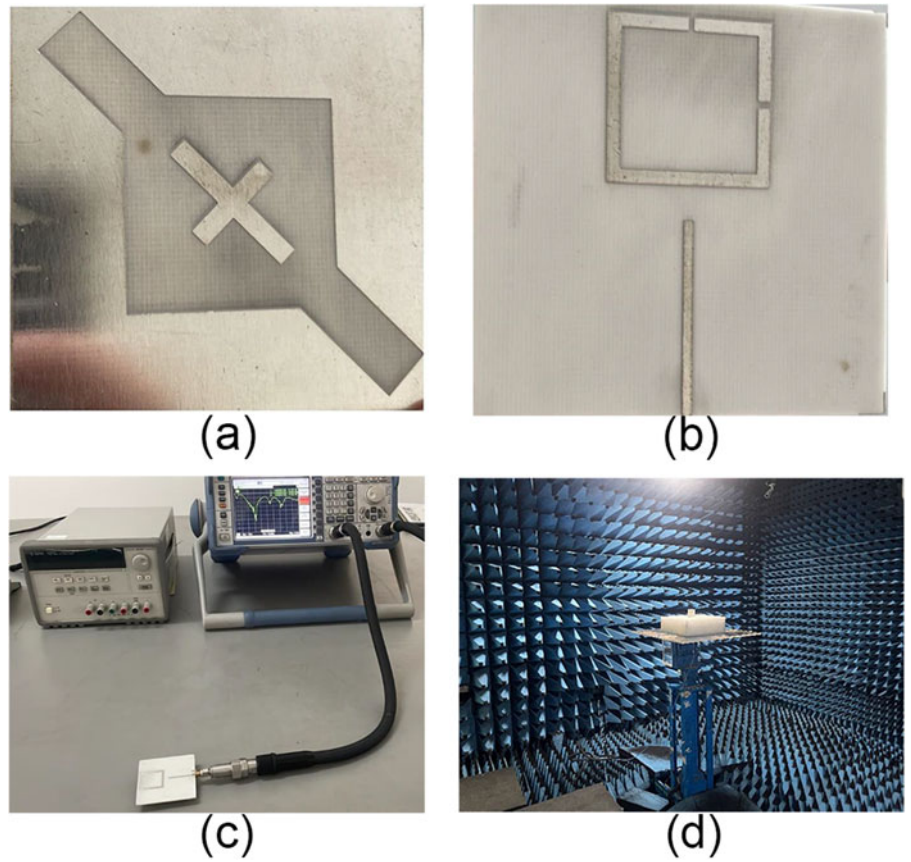


Figure 6. Fabricated antenna: (a) front view, (b) back view, (c) measuring S_{11} using VNA, and (d) antenna measured using anechoic chamber.

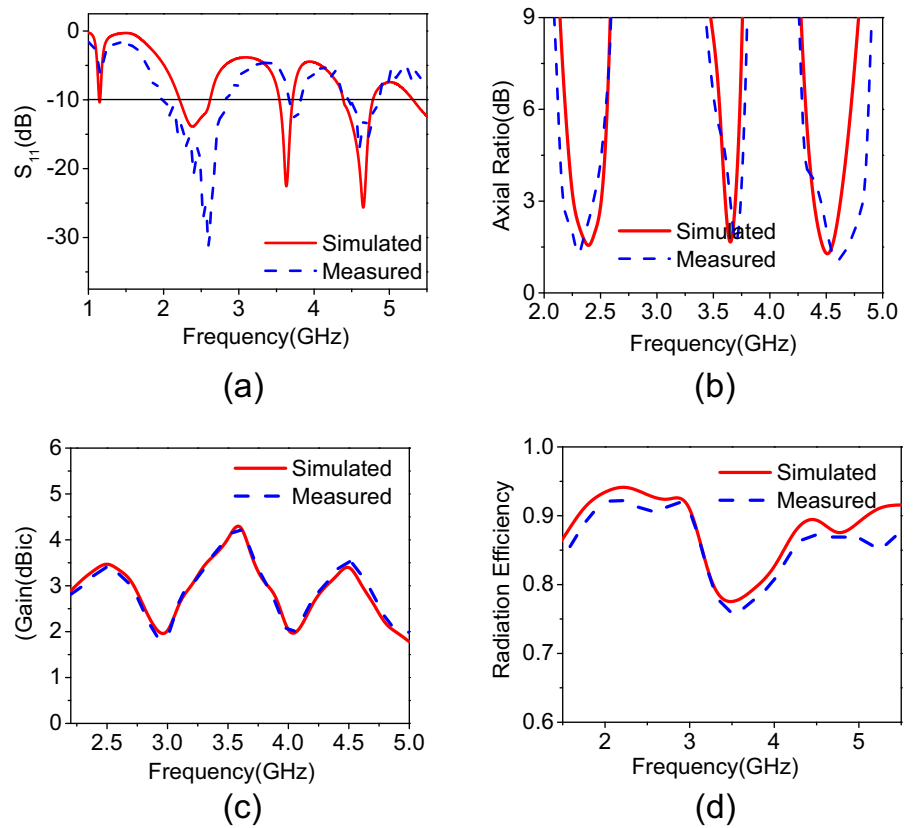


Figure 7. Comparison of simulated and measured results of (a) reflection coefficient (S_{11} dB), (b) axial ratio (dB), (c) gain (dB), and (d) simulated radiation efficiency.

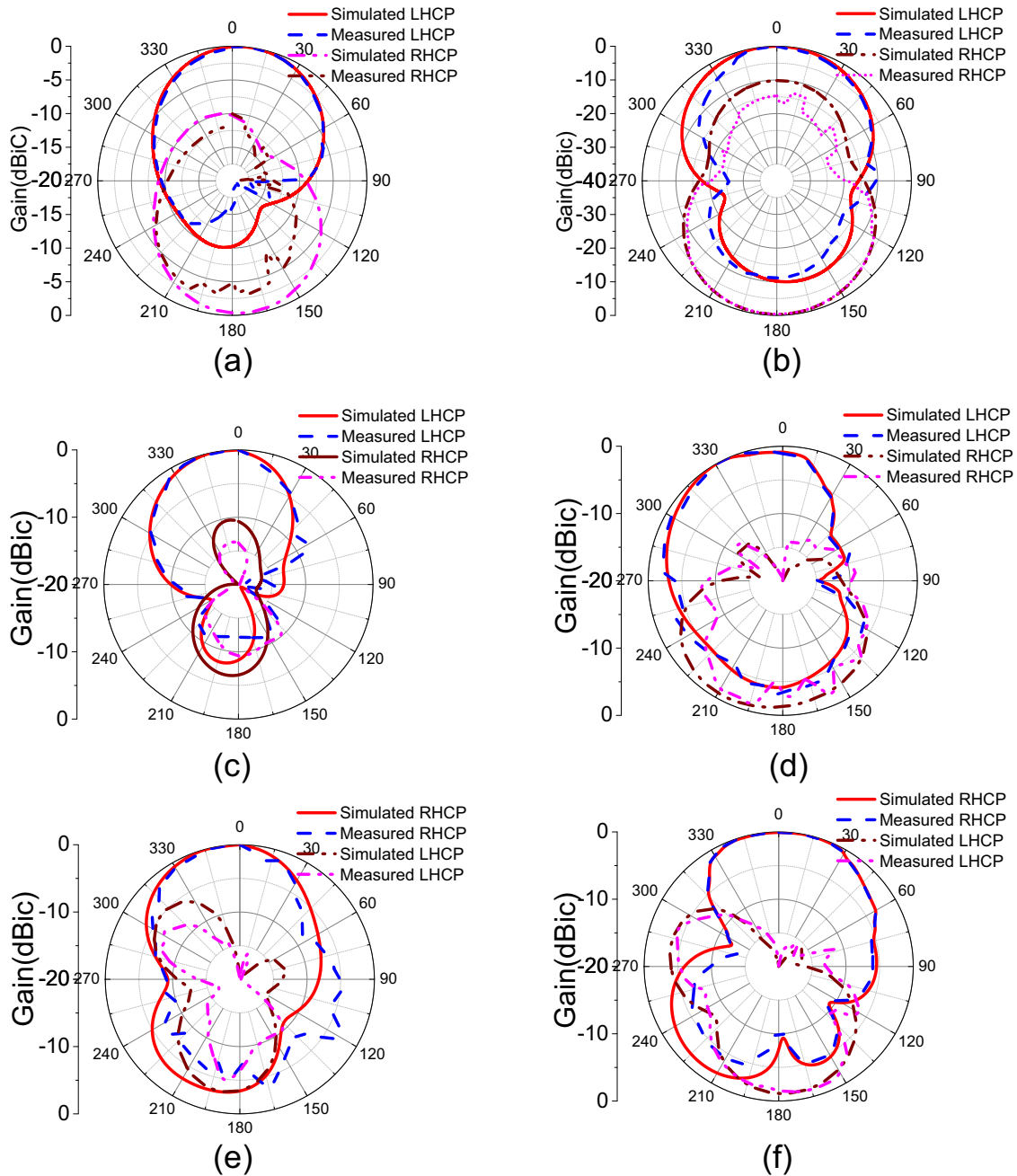


Figure 8. Radiation pattern of proposed antenna at 2.46 GHz (a) XZ plane and (b) YZ plane, at 3.67 GHz (c) XZ plane and (d) YZ plane, and at 4.6 GHz (e) XZ plane and (f) YZ plane.

Table 1. Supremacy of the proposed design with previous articles

[Ref]	Size ($\lambda_0 \times \lambda_0$)	*IBW (%)	ARBW (%)	Gain (dBic)	*ITFPS
[22]	0.38 × 0.38	17.8, 1.87, 8.63	LP antenna	4.64	Yes (using diodes)
[23]	0.1 × 0.17	22.69, 22.08, 16.03	LP antenna	2.72, 2.76, 2.89	Yes (using diodes)
[25]	0.52 × 0.52	22.3, 2.85, 2.17	LP antenna	4.4, 3.9, 3.8	Yes (using MTM units)
[26]	0.7 × 0.7	13.15, 14.88	3.2, 4.2	5.9, 6.1	Yes (using MTM units)
[27]	0.31 × 0.31	21.4, 12.8, 4.5	4.37, 11.9, 3.6	2.7, 4.2, 3.5	Yes (using MTM units)
[28]	0.95 × 0.95	64.54	11.76, 1.9, 3.87	2.88, 1.96, 2.96	Yes (using MTM units)
[Proposed]	0.4 × 0.4	31.68, 4.55, 8.6	13.04, 2.7, 8.6	3.7, 3.9, 3.8	Yes (using MTM units)

*IBW = impedance bandwidth, ITFPS = independent tuning of frequency bands and polarization sense.

and measured peak gain value of 3.8 dBic, 3.9 dBic, and 3.7 dBic is obtained at corresponding resonance frequencies, which are well in agreement and it is depicted in Fig. 7(c). The simulated radiation efficiency is shown in Fig. 7(d) and it is more than 80% in all frequency bands. The radiation pattern of the proposed design is shown in Fig. 8. The antenna is well radiating CP waves in the broadside direction showing clear evidence of dual polarization. LHCP is produced in the first and second band, while RHCP is produced in the third band. The cross-polarization level of minimum -10 dB is obtained with respect to co-polarization at all frequency bands. Figure 8(a) and (b) shows the radiation pattern at 2.42 GHz, Fig. 8(c) and (d) shows the radiation pattern at 3.67 GHz, and Fig. 8(e) and (f) shows the radiation pattern at 4.6 GHz. The supremacy of proposed design is compared with previous literature is provided in Table 1. It can be noted that the compactness, miniaturization, bandwidth, axial ratio, gain, and tunability of the design is comparable and superior than some of the references. The ARBW is good compared with [27] and [28]. The compact size is obtained when compared to all references cited in table except [27]. The gain is more in all bands compared to few references such as [23, 27] and [28].

Conclusion

The proposed structure is designed, simulated fabricated, and experimentally measured. The compact antenna radiates CP in three frequency bands with dual-sense polarization. The square slot antenna and SRR provides LHCP and cross strips gives RHCP. The measured impedance bandwidth of 770 MHz, 170 MHz, and 370 MHz are obtained in each band respectively. The ARBW of 300 MHz, 100 MHz, and 400 MHz are obtained and these are well agreement with simulated one. The peak gain of 3.8 dBic, 3.9 dBic, and 3.7 dBic is obtained along with radiation efficiency of 80%. The design is compact and well suitable for mobile and wireless application like the Bluetooth, n78 and n79 sub-6 GHz 5G applications, wherever CP is essential.

Acknowledgements. We thank Rogers Corporation for providing substrate materials to carry out fabrication of the design.

Competing interests. The author(s) declare none.

References

- Zhang JL, Da Liu Q, Wu QY, Ye LH, Li J-F and Wu D-L (2023) Dual-band vertically polarized omnidirectional patch antenna with low profile. *IEEE Antennas and Wireless Propagation Letters* **22**, 2881–2885. 10.1109/LAWP.2023.3303418
- Ambekar AG and Deshmukh AA (2022) Dual band compact square microstrip antenna for GSM and GPS applications. *Progress in Electromagnetics Research C* **118**, 99–112. 10.2528/PIERC21110504
- Ta SX, Phung TT, Nguyen KK and Nguyen-Trong N (2023) Low-profile dual-band tripolarized antenna using monopolar slotted patch. *IEEE Antennas and Wireless Propagation Letters* **22**, 2925–2929. 10.1109/LAWP.2023.3305374
- Viswambharan Anil Kumar C, Paul B and Mohanan P (2020) Compact triband dual F-shaped antenna for DCS/WiMAX/WLAN applications. *Progress in Electromagnetics Research Letters* **78**, 97–104. 10.2528/PIERL18062806
- Yang S, Xu J, Yu Z and Zhou J (2022) A tri-band shared-aperture antenna combining two sub-6G and one millimeter-wave bands with shared feeding port for 5G/B5G applications. *International Journal of RF and Microwave Computer-Aided Engineering* **32**, e23180. 10.1002/mmce.23180
- Li Y, Yang W, Xue Q and Che W (2024) A miniaturized dual-polarized tri-band antenna based on multimode and stacked scheme for multiband aperture-shared base-station applications. *IEEE Transactions on Antennas and Propagation* **72**, 4647–4652. 10.1109/TAP.2024.3383664
- Sharma M, Awasthi YK and Singh H (2019) Compact multiband planar monopole antenna for Bluetooth, LTE, and reconfigurable UWB applications including X-band and Ku-band wireless communications. *International Journal of RF and Microwave Computer-Aided Engineering* **29**, e21668. <https://doi.org/10.1002/mmce.21668>.
- Raj S, Mishra PK and Tripathi VS (2023) A multiband truncated patch antenna based on EBG structure for IoMT and 5G networks. *International Journal of Microwave and Wireless Technologies* **15**, 1745–1757. 10.1017/S1759078723000454
- Mishra P and Kulat KD (2023) Small-size multiband printed monopole antenna for wireless applications. *International Journal of Microwave and Wireless Technologies* **15**, 1801–1808. 10.1017/S1759078723000612
- Ezzahry B, Elhamadi T-E, Lamsalli M and Touhami NA (2023) New method based on genetic algorithm and Minkowski fractal for multiband antenna designs. *International Journal of Microwave and Wireless Technologies* **15**(8), 1–12. 10.1017/S1759078723001071
- Wu Y (2024) An optimized multiband antenna for UWB ad hoc networks based on topology optimization theory. *IEEE Transactions on Antennas and Propagation* **72**, 3896–3911. 10.1109/TAP.2024.3371537
- Seddiki ML, Nedil M, Tebache S and Hadji SE (2024) Compact multiband handset antenna design for covering 5G frequency bands. *IEEE Access* **12**, 20822–20829. 10.1109/ACCESS.2024.3362296
- Pietrenko-Dabrowska A and Koziel S (2024) Fast redesign of multiband antennas by means of orthogonal-direction geometry scaling and local parameter tuning. *IEEE Transactions on Antennas and Propagation* **72**, 6162–6167. 10.1109/TAP.2024.3369395
- Asif SM, Anbiyaei MR, Ford KL, O'Farrell T and Langley RJ (2019) Low-profile independently- and concurrently-tunable quad-band antenna for single chain sub-6 GHz 5G new radio applications. *IEEE Access* **7**, 183770–183782. 10.1109/ACCESS.2019.2960096
- Fabian-Gongora H, Martynyuk AE, Rodriguez-Cuevas J, Martinez-Lopez L, Martinez-Lopez R and Martinez-Lopez JI (2021) Independently tunable closely spaced triband frequency selective surface unit cell using the third resonant mode of split ring slots. *IEEE Access* **9**, 105564–105576. 10.1109/ACCESS.2021.3100325
- Hyun M, Sung Y and Kim E (2018) Hybrid square ring patch-slot antenna for dual-band circular polarized operation. *Microwave and Optical Technology Letters* **60**, 1052–1057. <https://doi.org/10.1002/mop.31093>.
- Tan Q and Chen F-C (2020) Triband circularly polarized antenna using a single patch. *IEEE Antennas and Wireless Propagation Letters* **19**, 2013–2017. 10.1109/LAWP.2020.3014961
- Yang Y, Qi Z, Chen Y and Li X (2024) Multi-band circularly polarized antenna for WLAN and WiMAX applications based on characteristic mode theory. *International Journal of Microwave and Wireless Technologies* **16**(1), 1–9. 10.1017/S1759078724000114
- Abdalrazik A, Goma A and Afifi A (2024) Multiband circularly-polarized stacked elliptical patch antenna with eye-shaped slot for GNSS applications. *International Journal of Microwave and Wireless Technologies* **16**(3), 1–7. 10.1017/S175907872400045X
- Nguyen-Trong N, Piotrowski A and Fumeaux C (2017) A frequency-reconfigurable dual-band low-profile monopolar antenna. *IEEE Transactions on Antennas and Propagation* **65**, 3336–3343. 10.1109/TAP.2017.2702664
- Luo Y, Zhao S, Yan N, An W and Ma K (2022) A frequency reconfigurable high-order mode monopole antenna with two independently controlled band. *International Journal of RF and Microwave Computer-Aided Engineering* **32**, e23333. 10.1002/mmce.23333
- Bharadwaj SS, Sibal D, Yadav D and Kishen Koul S (2020) A compact tri-band frequency reconfigurable antenna for LTE/Wi-Fi/ITS applications. *Progress in Electromagnetics Research M* **91**, 59–67. 10.2528/PIERM20011904

23. **Lin BXQ, Yu JW, Mei P, Jiang Y and Yu YQ** (2017) A highly integrated independently tunable triple-band patch antenna. *IEEE Antennas and Wireless Propagation Letters* **16**, 2216–2219. 10.1109/LAWP.2017.2707095
24. **Bai Q, Singh R, Ford KL, O'Farrell T and Langley RJ** (2017) An independently tunable tri-band antenna design for concurrent multiband single chain radio receivers. *IEEE Transactions on Antennas and Propagation* **65**, 6290–6297. 10.1109/TAP.2017.2748185
25. **Paul PM, Kandasamy K and Sharawi MS** (2017) A tri-band slot antenna loaded with split ring resonators. *Microwave and Optical Technology Letters* **59**, 2638–2643. <https://doi.org/10.1002/mop.30791>
26. **Kandasamy K, Majumder B, Mukherjee J and Ray KP** (2016) Dual-band circularly polarized split ring resonators loaded square slot antenna. *IEEE Transactions on Antennas and Propagation* **64**, 3640–3645. 10.1109/TAP.2016.2565729
27. **Paul PM, Kandasamy K and Sharawi MS** (2018) A triband circularly polarized strip and SRR-loaded slot antenna. *IEEE Transactions on Antennas and Propagation* **66**, 5569–5573. 10.1109/TAP.2018.2854911
28. **Tharehalli Rajanna PK, Rudramuni K and Kandasamy K** (2019) Compact triband circularly polarized planar slot antenna loaded with split ring resonators. *International Journal of RF and Microwave Computer-Aided Engineering* **29**, e21953. <https://doi.org/10.1002/mmce.21953>



Vinaya Kumar Sugganapalaya Rajanna received his B.E. degree in Electronics and Communication Engineering and M.Tech degree in VLSI and Embedded Systems Engineering from Visvesvaraya Technological University, Belgaum, Karnataka, India, in 2009 and 2011, respectively. He is currently working toward his Ph.D. in the dept. of Electrical and Electronics Engineering, Ghousia College of Engineering, Ramanagara, affiliated to VTU, Belgaum, Karnataka, India.

His field of research includes microelectronics, RF-VLSI, RFICs, MMICs, RF circuits, microwave engineering, and microstrip antennas.



Venkatesh T received his B.E. degree in Computer Science and Engineering from SJCIT, Karnataka, India, in 1995 and M.Tech in Computer Networks from SJCE, Mysore, India, in 1997. He received his Ph.D. in parallel computing and networks from Mysore University in 2016. He is currently working as a Professor in the dept. of Computer Science and Engineering at Ghousia College of Engineering, Ramanagara, India. His research interests are parallel computing, computer networks, computer

algorithms for antennas, and image processing algorithms.



Puneeth Kumar Tharehalli Rajanna received his B.E. degree in Telecommunication engineering and M.Tech degree in Digital Communication Engineering from Visvesvaraya Technological University, Belgaum, Karnataka, India, in 2009 and 2013, respectively. He received his Ph.D. from National Institute of Technology Karnataka, Surathkal, Mangalore, India, in 2020. He is currently working as an Assistant Professor in the dept. of Electronics and Telecommunication Engineering at Siddaganga Institute of Technology,

Tumkur. His field of research includes metamaterial-based antennas, leaky wave antennas, MMICs, RF circuits, microwave engineering, and microstrip antennas.



Shambulinga Mudukavvanavar received his B.E. degree in Electronics and Communication Engineering and M.Tech degree in Digital Communication Engineering from Visvesvaraya Technological University, Belgaum, Karnataka, India, in 2011 and 2013, respectively. He is currently working toward his Ph.D. in Electronics and Communication at R V College of Engineering, Bangalore, affiliated to VTU, Belgaum and Karnataka, India. His field of research includes

microstrip antennas, RF and microwave circuits, and image processing algorithms.